

CHAOTIC PULSES FOR DISCRETE REACTION DIFFUSION SYSTEMS

YASUMASA NISHIURA^{†¶}, DAISHIN UEYAMA[‡], AND TATSUO YANAGITA[†]

Abstract. Existence and dynamics of chaotic pulses on 1D lattice are discussed. Traveling pulses arise typically in reaction diffusion systems like the FitzHugh-Nagumo equations. Such pulses annihilate when they collide each other. A new type of traveling pulse has been found recently in many systems where pulses bounce off like elastic balls. We consider the behavior of such a localized pattern on 1D lattice, i.e., an infinite system of ODEs with nearest interaction of diffusive type. Besides the usual standing and traveling pulses, a new type of localized pattern, which moves chaotically on a lattice, was found numerically. Employing the strength of diffusive interaction as a bifurcation parameter, there appear route from standing pulse to chaotic pulse; intermittent type I and type III. If two chaotic pulses collide with an appropriate timing, it forms a periodic oscillating pulse called molecule. Interaction among many chaotic pulses is also studied numerically.

Key words. lattice differential equation, localized pulse, chaos, dissipative systems, bifurcation theory

AMS subject classification. 35B32, 35K57, 65P20, 65P30, 65P40

1. Introduction. We consider the dynamics of localized patterns on 1 dimensional lattice. In general, such a system is called a **Lattice Differential Equation (LDE)**. In fact, if the minimum spatial scale of the system is finite, it is natural to consider a model system on a lattice. There are many physical and biological examples which fall in this category such as [2, 7, 8, 10] for myelinated nerve axons and [5] for chemical reaction. The dynamics of LDE and its continuum counterpart are in general different and the aim of this paper is to present a new type of dynamic pattern called the **chaotic pulse** on one-dimensional diffusively coupled lattice with excitable nonlinearity. Chaotic pulses are localized patterns and behave chaotically in time as in Fig.1.1, which makes a sharp contrast with the usual standing or traveling ones for reaction diffusion systems on a continuum media.

A well-known example for such a difference is pinning (or propagation failure) for the following bistable scalar reaction diffusion equation on a lattice.

$$(1.1) \quad \frac{du_i}{dt} = f(u_i; a) + d(u_{i-1} - 2u_i + u_{i+1}), \quad i \in \mathbf{Z},$$

where $f(u; a) = u(1-u)(u-a)$, $0 < a < 1$ and u_i is a variable for the i -site. This may be regarded as a discretization of the continuum model

$$(1.2) \quad \frac{\partial u}{\partial t} = f(u; a) + Du_{xx}, \quad x \in \mathbf{R}.$$

It is known that the propagation speed of the frontal wave is uniquely determined by the parameter a , which increases monotonically as a function of a , and the sign of the velocity changes from negative to positive at $a = 1/2$. However, in fact, there exist

[†]Laboratory of Nonlinear Studies and Computations, Research Institute for Electronic Science, Hokkaido University, Kita-ku, Sapporo, 060-0812 Japan

[‡]Department of Mathematical and Life Sciences, Institute for Nonlinear Sciences and Applied Mathematics, Graduate school of Science, Hiroshima University, 1-3-1 Kagamiyama, Higashi-hiroshima, 739-8526 Japan

[¶]This research was supported in part by Grant-in-Aid for Scientific Research 16204008,14740225 and 15740063, Ministry of Education, Science and Culture, Japan

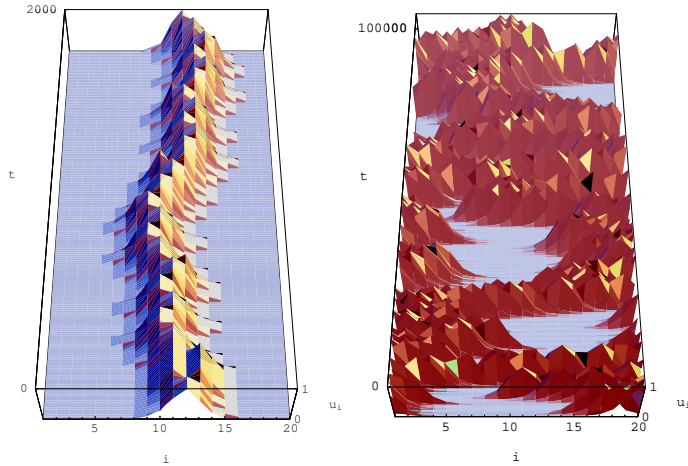


FIG. 1.1. A typical behavior of the chaotic pulse. ($\alpha = 0.305, k = 0.95, d = 0.12, n = 20$); (left): A birds-eye view plot for the chaotic pulse. (right): A long time behavior of the chaotic pulse.

some interval (a_-, a^+) in which the propagating speed of the frontal wave becomes 0 [7]. The small difference of size of basin is not enough to drive the interface. This phenomenon is called **pinning** (or propagation failure) that is not observed for the continuum model. In a continuous medium, any small difference can drive the interface, however in a discrete medium, the frontal wave can propagate if the parameter a exceeds some threshold.

This example shows that the discreteness somehow blocks the propagation and the steady states take over after that. On the other hand, for the system of equations like (2.1), the discreteness introduces a variety of dynamic patterns when the strength of diffusivities among lattice points is varied.

The content of the paper is the following. In Section 2 we introduce our model system. In Section 3 a phase diagram with respect to the diffusivity is studied and the mobility of chaotic pulse is also investigated. Bifurcational origin of chaotic pulse is clarified in Section 4 by using AUTO software. Interaction among many chaotic pulses is studied and several types of molecular states (time periodic patterns) are found numerically in Section 5. In Section 6 we show numerically that chaotic pulses converges to standing pulse when the grid size is decreased.

2. The model. In this paper we consider the following discrete reaction-diffusion systems with excitable kinetics on one-dimensional lattice. The model equations read

$$(2.1) \quad \begin{cases} \frac{du_i}{dt} = u_i(u_i - v_i^2 - \alpha) + d(u_{i-1} - 2u_i + u_{i+1}), \\ \frac{dv_i}{dt} = ku_i - v_i + \beta d(v_{i-1} - 2v_i + v_{i+1}), \end{cases} \quad i \in \mathbf{Z},$$

where d is the strength of the diffusion coupling between compartments, α, k are positive parameters and β is the ratio of diffusivities. The model (2.1) could be

regarded as a coarse discretization of the following continuous model.

$$(2.2) \quad \begin{cases} \frac{\partial u}{\partial t} = u(u - v^2 - \alpha) + Du_{xx}, \\ \frac{\partial v}{\partial t} = ku - v + \beta Dv_{xx}, \end{cases} \quad x \in \mathbf{R},$$

where D is the diffusion coefficient, however we study (2.1) as an independent model, not an approximation of (2.2). The model (2.2) called the **P-model** was introduced in [11] as a minimal model that shows self-replicating patterns of propagating type. Here we quickly review the main features of (2.2). First note that $(u, v) = (0, 0)$ is locally stable as a solution to (2.2), we add a perturbation of finite size to observe nontrivial patterns. In fact, starting from a localized initial data like step function, (2.2) shows a variety of dynamic patterns, such as standing pulse, traveling pulse and self-replicating pattern. One of the remarkable properties of (2.2) is that traveling pulses satisfy the preservation at head-on collision, namely they do not annihilate and emit two counter-propagating waves after collision which makes a sharp contrast with those of the FitzHugh-Nagumo equations. It is known that such a property holds for a class of reaction diffusion systems including the Gray-Scott model. Originally, the P-model was introduced for the study of self-replicating dynamics from a global bifurcational view point. For one-dimensional case, [11] showed a hierarchy structure of saddle-node bifurcation points which drives self-replicating dynamics.

Although it is interesting to compare the dynamics of (2.1) with that of (2.2) (in fact we come back to this issue in Section 6), we shall study the dynamics of localized patterns on a lattice and its d -dependency, especially we focus on the chaotic pulses. It should be remarked that our chaotic pulse is essentially different from the well-known chaos arising in the forward time discretization of the logistic equation, namely t -direction remains continuous for our model and the kinetics (see the Section 2.1) does not have any chaotic dynamics.

2.1. ODE dynamics of the model. The corresponding ODE kinetics of the discrete P-model (2.1) is given by

$$(2.3) \quad \begin{cases} \frac{du}{dt} = u(u - v^2 - \alpha), \\ \frac{dv}{dt} = ku - v. \end{cases}$$

Two positive parameters α and k control the ODE dynamics. Note that (2.3) has a stable critical point $(u, v) = (0, 0)$ independent of the parameters. The phase diagram with respect to these parameters and typical flows are drawn in Fig.2.1. A bifurcation diagram with respect to α for fixed $k = 0.95$ is depicted in Fig.2.2. For appropriately large α the system behaves like an excitable system with $(0, 0)$ being a rest state. As α is decreased, two nontrivial critical points (upper one is a stable focus and lower one is a saddle) emerge through the saddle-node bifurcation as in Fig.2.2. The upper branch loses its stability through the Hopf bifurcation at H_0 . For definiteness we fix the parameters as $k = 0.95$ and $\alpha = 0.305$ throughout the paper.

2.2. Computational setting. For numerical purpose we compute the discrete P-model (2.1) under periodic boundary conditions, namely we consider the following

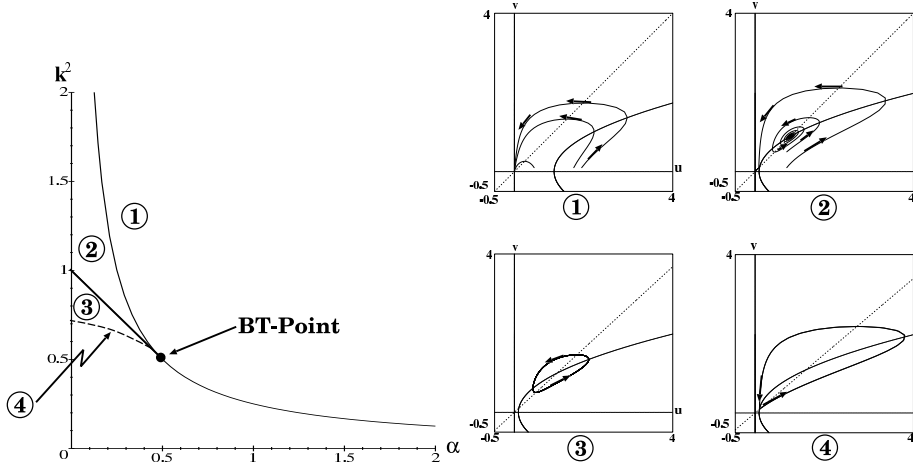


FIG. 2.1. (left): There is a Bogdanov-Takens (BT) singularity at $(\alpha, k^2) = (1/2, 1/2)$ in the parameter space (α, k^2) . The thin line denotes the saddle-node bifurcation point, and thick line denotes the Hopf bifurcation point. A BT-point is a singularity of codim 2 where saddle-node and Hopf bifurcations merge. The dotted line denotes the homoclinic bifurcation. (right): The number for each figure indicates the regime in the parameter space.

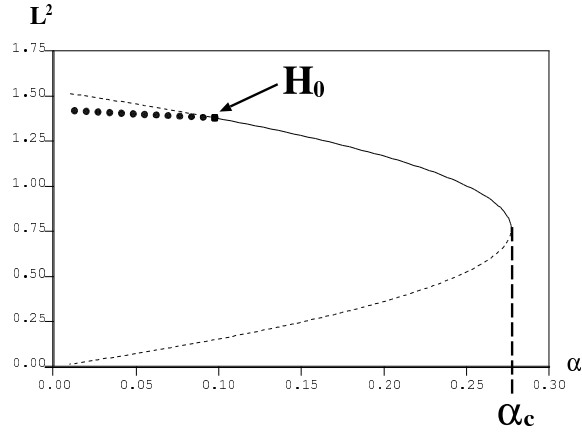


FIG. 2.2. The bifurcation diagram for $k = 0.95$. The Saddle-Node bifurcation occurs at α_c and the supercritical Hopf bifurcation occurs at H_0 . Vertical axis shows L^2 norm.

system for finite n .

$$(2.4) \quad \left\{ \begin{array}{l} \frac{du_i}{dt} = u_i(u_i - v_i^2 - \alpha) + d(u_{i-1} - 2u_i + u_{i+1}), \\ \frac{dv_i}{dt} = ku_i - v_i + \beta d(v_{i-1} - 2v_i + v_{i+1}), \\ u_{n+1} = u_1, u_0 = u_n, v_{n+1} = v_1, v_0 = v_n. \end{array} \right. \quad i = 1, \dots, n,$$

For large n , the dynamics of the localized pulse of (2.4) is essentially the same as that of (2.1), since the tail of the pulse decays exponentially. In fact the main body of the pulse treated here occupies 6 to 9 grid points. In the sequel we take $n = 20$,

which is enough for our purpose since all the qualitative behaviors and statistical characteristics do not change even if n is increased to 100. We fix $\beta = 4$ as well as $\alpha = 0.305$ and $k = 0.95$, and employ d as a bifurcation parameter. Our goal is to show the existence of a localized pulse moving around chaotically when d is taken appropriately, and to study the route to such a chaotic pulse with respect to d .

We use the fourth order Runge-Kutta method for solving (2.4) throughout the paper. Note that we confirm that our results do not depend on the numerical methods, namely other schemes such as Euler, eighth order Runge-Kutta and fifth order Runge-Kutta with adaptive step size control method show qualitatively the same results.

3. Phase diagram for the discrete P-model. We present a variety of dynamic patterns of pulses for the discrete P-model as d is varied. Since $(u, v) = (0, 0)$ is locally stable in LDE sense, we add a perturbation of finite size to it to obtain nontrivial patterns. For instance the following initial data was employed to make the phase diagram.

$$\begin{cases} u_i = 1 + \eta, & v_i = 0.8 + \eta, & 1 \leq i \leq 5, \\ u_i = 0, & v_i = 0, & 6 \leq i \leq 20, \end{cases}$$

where the $\eta \in [-0.01, 0.01]$ is a small random disturbance. The phase diagram and the corresponding space-time plots are depicted as Fig.3.1. The **standing pulse** (a)(f) and the **traveling pulse** (d) are also observed in the continuous model (2.2), however the **shaking pulse** (b)(e) and the **chaotic pulse** (c) are observed only for the discrete P-model. The shaking pulse is a time-periodic solution rolling from side to side. The chaotic pulse moves chaotically with keeping its localized structure and it is a notable dynamic pattern arising only for the discrete system. Such a chaotic pulse should be distinguished from the well-known spatio-temporal chaos arising in, for instance, the Kuramoto-Sivashinsky equation in which chaotic state is not localized. The number of compartments n must be appropriately large enough for our purpose, since we make all simulations on a bounded circle (recall the periodic boundary conditions) and the distinction between **localized pulse** and **pulse train** becomes unclear for small n , in fact $n = 8$ is not large enough for such a distinction.

3.1. The chaotic pulse. The chaotic pulse is observed in the parameter regime from $d = 0.117$ to 0.1305 . The typical motion of the chaotic pulse is shown in Fig.1.1. As you can see, the chaotic pulse changes its position irregularly. It is confirmed numerically that the chaotic behavior is **not** a transient phenomenon in the sense that it persists more than $t = 10^8$ for several parameter values including the case Fig.1.1 (right). In the following subsections we present two more evidence to support our claim.

3.2. Sensitive dependence on initial conditions. We computed the sensitive dependence of the chaotic pulse starting from slightly different two initial data. Fig.3.2 shows 2 simulations in which the difference of initial data is only 10^{-5} for the u -component. As is easily seen, two orbits becomes almost independent at $t = 2000$, which strongly indicates the sensitive dependence on initial data.

We also computed the **maximum Liapunov exponent** numerically as depicted in Fig.3.3. There exists an interval from $d = 0.117$ to 0.1305 in which the exponent is positive. This interval corresponds exactly to the parameter regime where we observe the **chaotic pulse** (see also Fig.3.1). The exponent is almost equal to zero on both sides of the chaotic regime which indicates the existence of time-periodic solutions. In fact those time-periodic solutions are **shaking pulses** and **traveling pulses** respectively as in Fig.3.1(b)(d)(e). Recall that shaking pulses are not observed for the continuous P-model. It should be noted that the region around $d = 0.1931$ has a positive maximum Liapunov exponent. The value $d = d_{ct} = 0.1931$ matches the transition point where the shaking pulse changes into the traveling pulse. Numerics tells us that the shaking pulse approaches a heteroclinic orbit connecting two unstable standing pulses as d tends to $d = d_{ct}$ from above (see Fig.4.7 and its caption), so that the period of which goes to infinity at the same time. When d passes the transition point, the orbit changes to the traveling pulse which stays quite a long time near those unstable standing pulses. Such a transition makes the Liapunov exponent positive. The main reason for the positivity of the maximum Liapunov exponent around $d =$

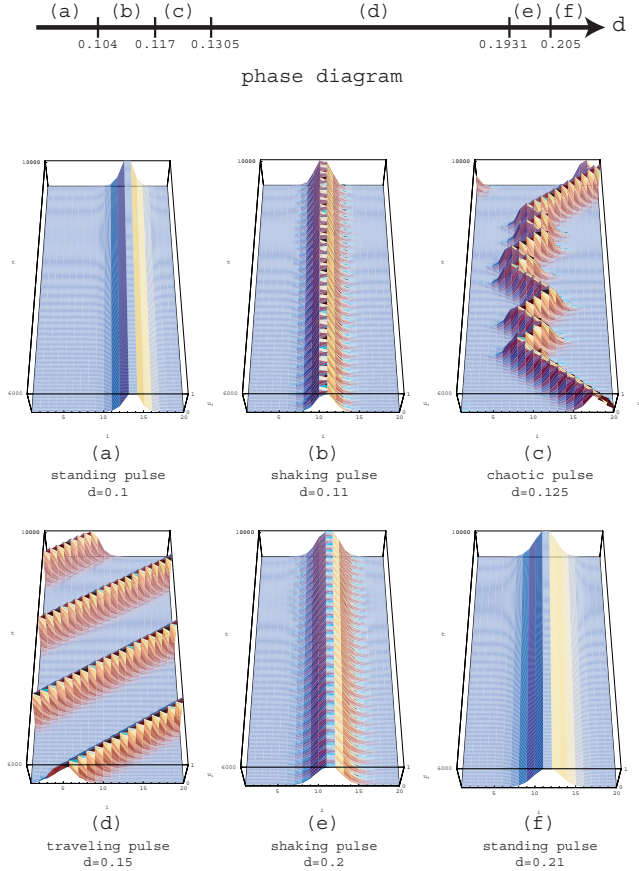


FIG. 3.1. Phase diagram for the discrete P -model with 20 compartments subjected to periodic boundary conditions ($\alpha = 0.305, k = 0.95, n = 20$); (above): Birds-eye view plots for each phase are shown (below): (a)(f) Standing pulse. (b)(e) Shaking pulse. Shaking pulses are time-periodic solutions rolling from side to side. (c) Chaotic pulse. The chaotic pulse moves chaotically with keeping its localized structure. (d) Traveling pulse. The traveling pulse moves in one direction with a constant speed. By symmetry there exists a traveling pulse moving in opposite direction simultaneously.

Animation files are supplied. (a)0100.mov, (b)0110.mov, (c)0125.mov, (d)0150.mov, (e)0200.mov, (f)0210.mov.

d_{ct} is subjected to our choice of algorithm. We calculate the maximum Liapunov exponent in the following way (the method is described in e.g. [14, 15, 16]): Consider two orbits, a "reference" orbit and a "test" orbit, separated at time t_0 by a small distance d_0 in phase space. The distance of the two orbits may (or may not) stretch as time is increased. We estimate the maximum Liapunov exponent as a measure of the rate of above separation. This simple algorithm causes the positivity of the maximum Liapunov exponent near the critical point $d = d_{ct}$, because of the existence of separatrix as in Fig.3.4, in fact the smaller the size of perturbation d_0 , the narrower the size of positive region. It is an advantage of such an algorithm to allow us to detect

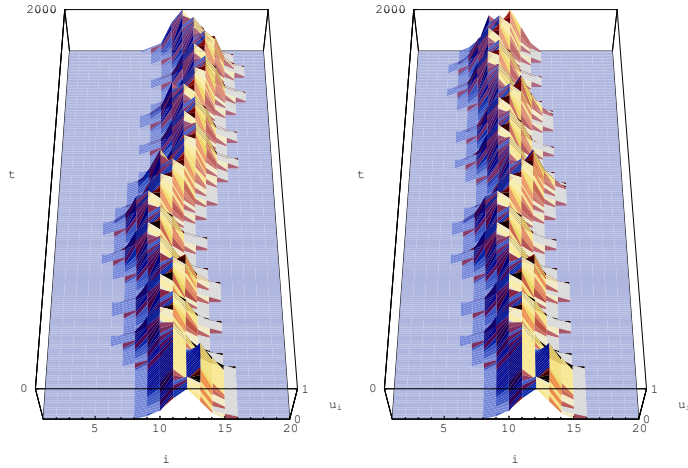


FIG. 3.2. The birds-eye view plots for the 2 different orbits started from slightly different initial data. The small difference grows in time exponentially, and the dynamics are almost independent at $t = 2000$. ($\alpha = 0.305, k = 0.95, d = 0.12, \beta = 4, n = 20$)

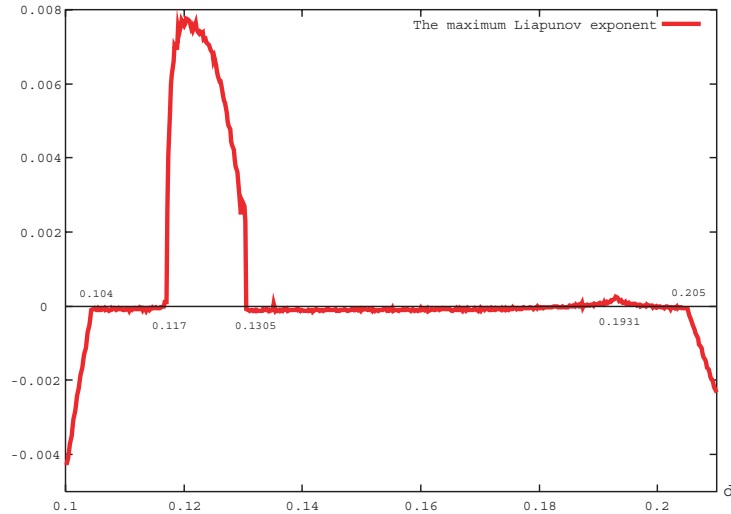


FIG. 3.3. The maximum Liapunov exponent for the pulse arising in the discrete P -model. ($\alpha = 0.305, k = 0.95, n = 20$)

the heteroclinic orbit at $d = d_{ct}$ (see Fig.3.4 and its caption).

3.3. Statistical analysis of the mobility of the chaotic pulse. A natural question is whether the motion of the chaotic pulse is of **Brownian motion** type or not. To get a statistical distribution of the chaotic pulse, we define the pulse position $I_{max}(t)$ by the lattice site i at which $u_i(t)$ takes the maximum value on the whole lattice. We study an ensemble of the positions of the chaotic pulses for the set of tiny

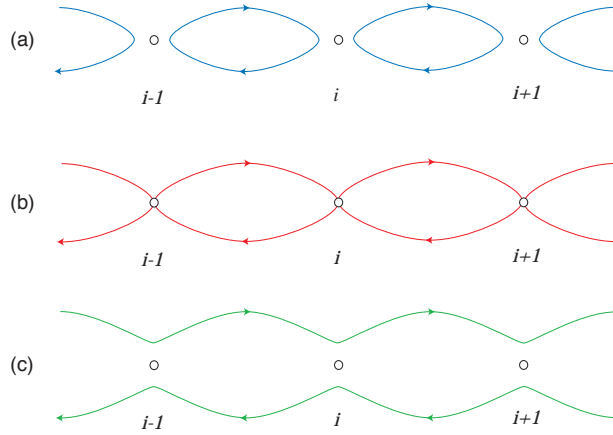


FIG. 3.4. Schematic illustrations for the transition from shaking pulse to traveling pulse near d_{ct} . The white disk stands for the unstable standing pulse and its arbitrary translation produces infinitely many standing pulses on a lattice. Here we superpose those pulses on the same plane. (a): For the case of $d > d_{ct}$, the shaking pulse is time-periodic and forms a blue color circle. (b): For the case of $d = d_{ct}$, the heteroclinic orbit connecting two unstable standing pulse emerges. The red curve indicate the heteroclinic orbit connecting two unstable standing pulse solutions. (c): For the case of $d < d_{ct}$, the above heteroclinic orbits are tied together to create a traveling pulse (green curve). The behavior of pulse is drastically changed near d_{ct} , namely it remains within a finite interval (shaking pulse) or goes away to infinity (traveling pulse), which causes the positivity of the Liapunov exponent.

different initial conditions at a given time. We employ the following initial conditions:

$$\begin{cases} u_i = 1 + \eta, & v_i = 0.8 + \eta, & 1 \leq i \leq 2, \\ u_i = 0, & v_i = 0, & 3 \leq i \leq 20, \end{cases}$$

where η is uniformly distributed random number $\eta \in [-0.001, 0.001]$. For a sufficiently large T , the statistical distribution of the position of the chaotic pulse at given time T turns out to be **Gaussian** as shown in Fig.3.5. We also calculated the kurtosis for each distribution by changing the parameter d as in Fig.3.6. The kurtosis ν is computed by dividing the fourth central moment by the square of the variance of the data:

$$(3.1) \quad \nu = \frac{\langle (I_{max}(T) - \langle I_{max}(T) \rangle)^4 \rangle}{\langle (I_{max}(T) - \langle I_{max}(T) \rangle)^2 \rangle^2}.$$

Except near the critical points ($d = 0.117$ and $d = 0.1305$ respectively), kurtosis is almost 3 which indicates a **Gaussian distribution** and expects that a chaotic pulse behaves like a **normal diffusion process**. We also calculated the standard deviation of the distribution which gives a diffusion coefficient of a chaotic pulses as is plotted in Fig.3.7.

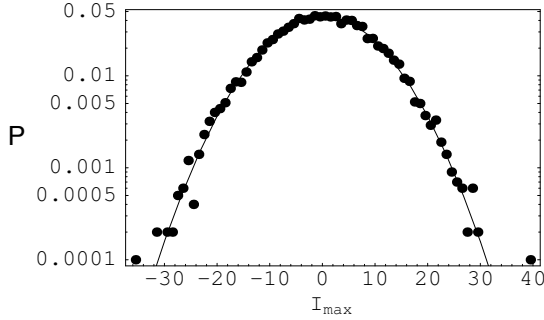


FIG. 3.5. *Distribution of position for the chaotic pulse ($d = 0.12$). Starting from many different initial conditions, the statistical distribution of the position $I_{max}(T)$ for the chaotic pulse at $T = 10^4$, is depicted. Except near the critical parameter region, quadratic form of the distribution with semi-log plot indicates a **Gaussian distribution**. Indeed, the kurtosis of distribution in a chaotic regime is close to 3 as in the next figure.*

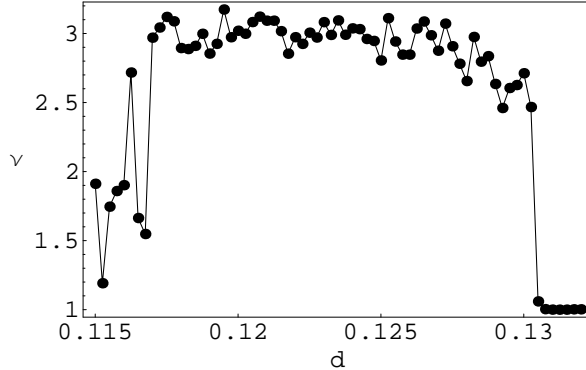


FIG. 3.6. *The kurtosis of distribution of position for the chaotic pulse. The kurtosis is approximately equal to 3 except near the critical points. This means the motion of chaotic pulses can be regarded as a **Brownian motion**, although the motion is governed by the deterministic dynamics.*

4. Route to chaos. One of the main issues is to clarify how the chaotic pulse emerges from the time-periodic or the traveling pulse solution. As was observed in Section 3, there are two transition points: one is in between (b) and (c) in Fig.3.1 and the other is in between (c) and (d) in Fig.3.1. At the former transition point denoted by $d = d_{c1}$, the shaking pulse suddenly change into the chaotic pulse when d is increased. For the latter case, when d is decreased, the traveling pulse suddenly change into the chaotic pulse at $d = d_{c2}$. Numerics shows that $d_{c1} \approx 0.117$ and $d_{c2} \approx 0.1305$ respectively. It is useful to recall that there are three types of route from time-periodic state to the chaotic one:

- Intermittency,
- Period doubling,
- Break up of torus.

Fig. 4.1 shows the typical behaviors right after the parameter d enters the chaotic regime. In the left figure ($d = 0.1172 > d_{c1}$) the pulse behaves like a shaking pulse for a while, but suddenly bursts, i.e., moves to the right or left for a short time, then returns

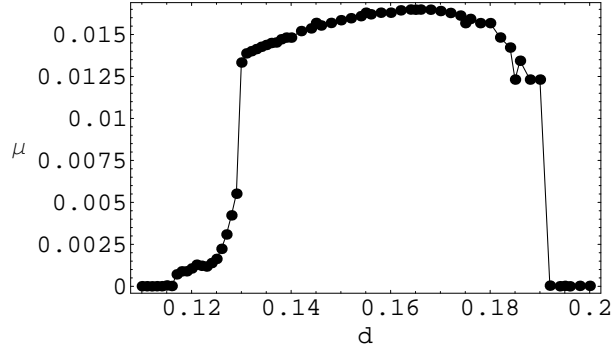


FIG. 3.7. The standard deviation of the pulse position at a given time is plotted for various d -values. For the traveling pulse regime, μ gives its averaged speed which is consistent with the result of AUTO (see Fig.4.7). Apart from the critical values, the distribution is almost Gaussian indicating that the motion of the chaotic pulse can be regarded as normal diffusion process. For the chaotic pulse regime, the diffusion coefficient is estimated from standard deviation.

again to shaking motion. In the right figure ($d = 0.1304 < d_{c2}$) the pulse behaves like a traveling wave for most of time, however it changes the direction unpredictably. Both simulations strongly suggest the emergence of the chaotic pulse via intermittency. In the following subsections, we will show that intermittency is responsible for the onset of chaotic pulses by two different approaches: one is the statistical analysis and the other is to compute the global behavior of solution branches such as shaking and traveling pulses with respect to d .

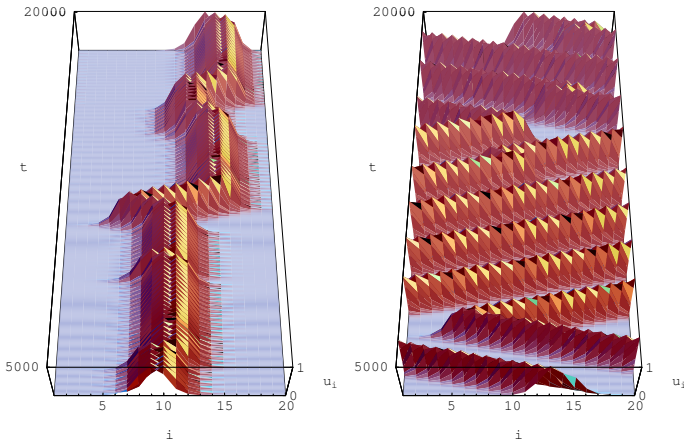


FIG. 4.1. Two types of intermittent behaviors of chaotic pulses. ($\alpha = 0.305, k = 0.95, n = 20$); When d enters into the chaotic regime, but close to the transition point, the orbit undergoes intermittency, namely it behaves like an ordered pattern (laminar state) for most of time, but interrupted unpredictably (burst state). The laminar state for $d = 0.1172 > d_{c1}$ (left): (resp. $d = 0.1304 < d_{c2}$ (right):) is shaking pulse (resp. traveling pulse).

Animation files are supplied. (left)01172.mov, (right)01304.mov.

4.1. Intermittency. Dynamic behavior of the chaotic pulse at the edge of the chaos regime has a special feature, namely it inherits the ordered dynamics from just outside of the chaotic regime, but interrupted in an unpredictable way. In fact, if $d < d_{c1}$, the solution remains as a shaking pulse, but once d enters into the chaotic regime $d > d_{c1}$, the solution behaves like a shaking pulse for almost all time except the sudden interruptions as in Fig.4.1 (left). A similar thing happens also at the right edge of the chaotic regime $d \approx d_{c2}$. In this case, the ordered state is the traveling pulse observed for $d > d_{c2}$. When d is decreased and becomes smaller than d_{c2} , then the orbit behaves like a traveling pulse but changes its direction intermittently like Fig.4.1 (right). Generally, these routes to chaos of intermittent type are classified as follows[17]:

- Type I : saddle-node bifurcation,
- Type II : Hopf bifurcation,
- Type III : inverse period doubling bifurcation.

In the following two subsections, first we compute the characteristic exponents and detect which type of intermittency actually occurs. Second we compute the solution branches globally of the ordered states such as standing pulse, shaking pulse and traveling pulse, and clarify the origin of intermittency from a bifurcational view point.

4.2. Route to chaos through intermittency – Statistical viewpoint –.

In order to quantify the interruption of the laminar state by the burst state, first we introduce the following $\sigma(t)$:

$$(4.1) \quad \sigma(t) = \Theta(|I_{max}(t - \delta t) - I_{max}(t)| - x_c),$$

where Θ is the Heviside function, δt is appropriate time interval and x_c is some positive constant. $\sigma(t)$ is a characteristic function for the burst state, i.e., $\sigma(t) = 1$ for burst state and where $\sigma(t) = 0$ for laminar state. Using $\sigma(t)$, we calculate the set of duration time $\ell = \{l_1, l_2, \dots, l_N\}$ of the laminar state, where each element measures how long the laminar state lasts. Here N is the number of the laminar state for some finite time interval. The definition of ℓ is following.

$$(4.2) \quad \ell = \{t_2 - t_1 | t_1 < t_2, \forall t \in [t_1, t_2] \text{ s.t. } \sigma(t) = 0\}.$$

Using $\sigma(t)$, the time series of laminar and burst states is visualized like Fig.4.2. It is clearly seen that the burst state appears intermittently after a long time duration of the laminar state.

In Fig.4.3, the parameter dependency of the mean duration time for the laminar state is calculated. The power law dependency of the parameter $\epsilon = \frac{|d_c - d|}{d_c}$ is clearly seen indicating the emergence of the **Type I intermittent chaos** at the critical point $d_{c1} = 0.117$ [12, 13]. Exactly the same computation for the laminar length l near the critical value $d_{c2} = 0.1305$ yields to Fig.4.4. The result strongly suggests that the transition from the traveling pulse to the chaotic pulse is the **Type III intermittency**.

It should be noted that there exists some difficulty around the transition point $d = d_{c2}$, namely the duration time of the laminar state becomes longer as the parameter d being closer to the critical point of the emergence of the intermittent chaos. This fact makes it difficult to classify the solution into chaotic state or ordered state according to its evolutionary behavior. In order to distinguish these behaviors, we

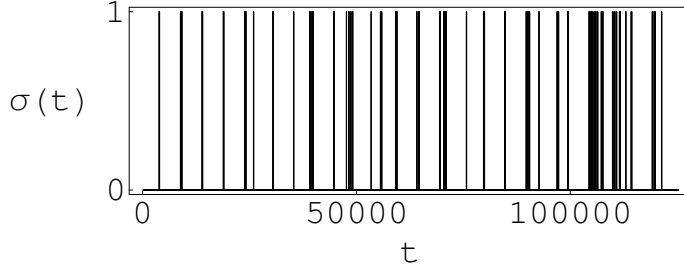


FIG. 4.2. Time series $\sigma(t)$ of the Type I intermittency ($d = 0.11715$). Time series of a binary representation of a laminar and a burst state is shown. The black line represent a burst state. For 'quasi-shaking' state and sudden shift of the position corresponds to laminar and burst state respectively. The statistical results do not sensibly depend on the choice of the critical value.

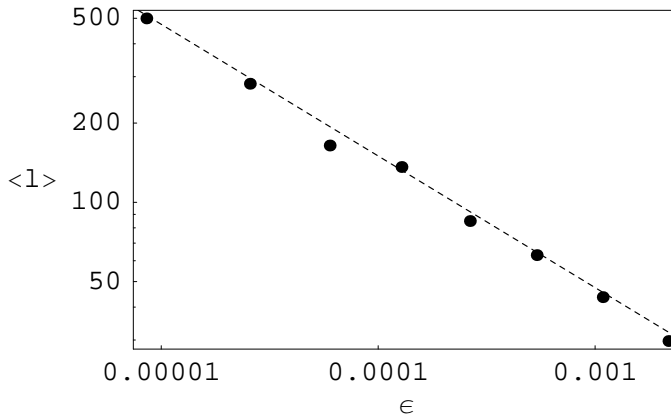


FIG. 4.3. The time averaged length $\langle l \rangle$ of a laminar state v.s. distance ϵ from the critical transition point d_{c1} . This characteristics is common for the Type I intermittent chaos. The parameter dependency of the mean duration time of the laminar state near critical value $d_{c1} = 0.117$ is plotted. The power law dependence of the mean duration time of laminar state is clearly observed. The index of the power law is almost $-1/2$ which indicate the Type I intermittency and the critical value is consistent with the result of Fig. 4.7.

define the following probability $Q(d; T_1, T_2)$ measuring how frequently chaotic behaviors are observed for given d and T_1 . When the duration of unidirectional motion of pulse exceeds T_1 within a long time evolution $T_2 > T_1$, we regard the state of pulse as a non-chaotic state, otherwise, the state of pulse being regarded as a chaotic one. Although the state of the pulse depends on an initial condition, T_1 and T_2 respectively, the probability (or frequency) $Q(d; T_1, T_2)$ is calculated starting from many different initial conditions (Fig.4.5). As T_1 is increased, the transient behavior dies out and the probability $Q(d; T_1, T_2)$ must be decreased below the critical values $d = d_{c2}$. Indeed, $Q(d; T_1, T_2)$ is almost zero for a larger T_1 , and this means that the state of pulse is attracted to a periodic state for almost all initial conditions. Furthermore, there exists a parameter region $d \in (0.1305, 0.1306)$ where the long time chaotic behaviors are observed with a finite probability. However, these states are transient because the probability of chaotic pulse tends to zero as T_1 is increased.

4.3. Route to chaos through intermittency – Global bifurcation view point –. Using the AUTO software [4], we study the global behaviors of standing,

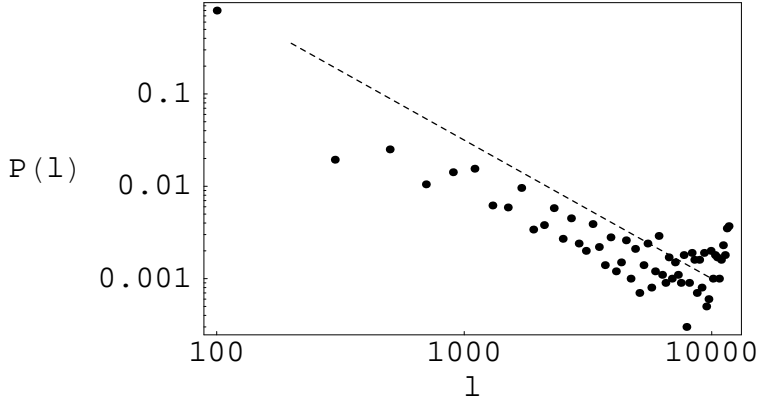


FIG. 4.4. The statistical distribution of laminar length l near the critical value $d_{c2} = 0.1305$ shows power law, dotted line shows $-3/2$ slope. The $-3/2$ exponent indicates the Type III intermittency.

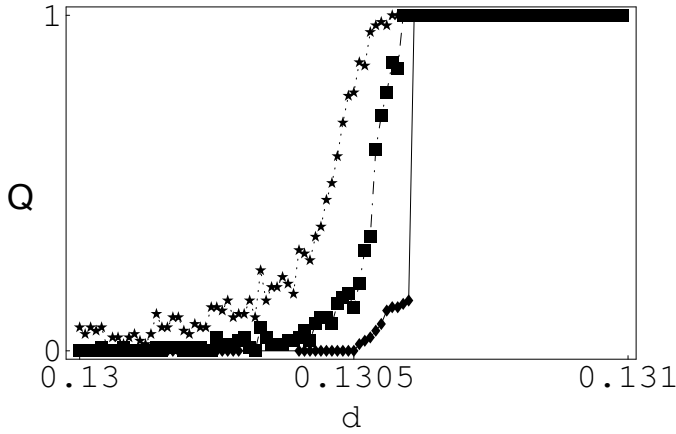


FIG. 4.5. Dependency of $Q(d; T_1, T_2)$ on d (Star sign: $T_1 = 15000$, Filled square: $T_1 = 20000$, Filled diamond: $T_1 = 100000$). As T_1 is increased, the transition curve approaches a step function indicating that there is a transition point near $d = 0.1305$. See the text for definition for $Q(d; T_1, T_2)$ and T_1 .

shaking, and traveling pulses with respect to d . The grid number is fixed to be $n = 20$. To begin with, we pursue the branch of standing pulses. What we have to do first is to find a seed solution from which we can trace the branch. By solving the discrete P-model numerically, we can obtain such a solution say at $d = 0.08$, then AUTO allows us to obtain the global bifurcating branch for the 1 hump standing pulse solution as in Fig.4.6. There exists a curve that corresponds to the 1 hump standing pulse solution. The solid (resp. dotted) line shows the **stable** (resp. **unstable**) standing pulse solution respectively. There are two Hopf bifurcation points HP1 and HP2 from which time-periodic shaking pulses emanate. Note that there are two subintervals in

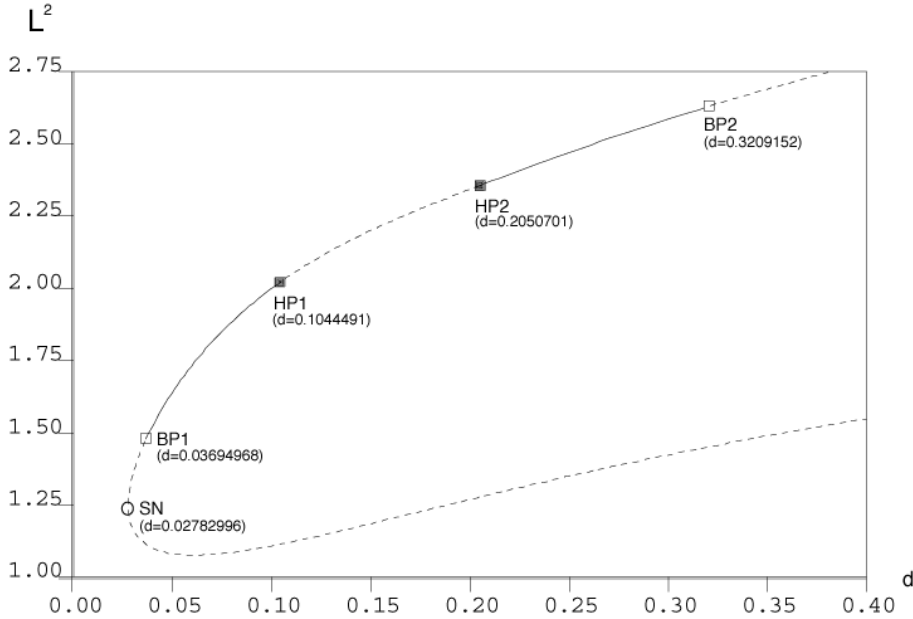


FIG. 4.6. The global bifurcation diagram for the 1 hump standing pulse solution with respect to d for the discrete P -model ($n = 20$). A solid line shows the **stable** stationary solution and dashed line shows the **unstable** stationary solution respectively. There are 5 bifurcation points on the curve. $HP1$ and $HP2$ stand for the Hopf bifurcation points, $BP1$ and $BP2$ for other types of bifurcation points, and SN for the saddle-node bifurcation point. The bifurcation diagram says that the stable 1 hump standing pulse solution exists in between $d = 0.036$ and $d = 0.104$, also between $d = 0.205$ and $d = 0.32$. The results are consistent with the results obtained by numerical simulations (see also Fig.3.1). The limitation of the number of the compartments is responsible for the emergence of $BP2$, in fact, for larger d , the width of a pulse becomes wider, which causes the number of the compartment supporting the pulse shape becomes larger, and eventually fills the ring. If the number of the compartments becomes infinite, $BP2$ does not appear.

which stable standing pulse solutions exist, i.e., the interval between $BP1$ and $HP1$, $HP2$ and $BP2$ respectively, which is consistent with the phase diagram in Fig.3.1.

The next step is to trace the bifurcating time-periodic solutions and clarify the emergence of chaotic pulses from bifurcational view point. The global behaviors of traveling solutions as well as two Hopf branches (shaking pulses) emanating from $HP1$ and $HP2$ are depicted in Fig.4.7. The vertical axis shows the **period of the solution**. The period of the traveling solution is the total time for the pulse to travel on the ring. The period of the shaking pulse solution is the duration of deformation necessary for one cycle. The black disk (resp. the white disk) corresponds to stable (resp. unstable) periodic solution. The branch of shaking pulse from $HP1$ turns back and loses its stability at the saddle-node point (see SN point at $d = 0.117105$). If d becomes slightly larger than SN , the chaotic pulse is observed, which indicates that the chaotic pulse emerges at the SN point through the **Intermittency Type I route**[12]. Actually, we see a clear evidence of the aftereffect of the saddle-node point in the time evolution of Fig.4.1 (left). Furthermore recall that the statistical quantity also supports the conclusion (see Fig.4.3).

On the other hand, the period of shaking pulses emanating from $HP2$ becomes longer and longer and eventually the continuation procedure fails at MX point ($d = 0.1931$) due to its long period. The MX point is very close to the value of the critical

point where the shaking pulse changes to the traveling pulse. In fact, by careful numerical simulations, we see that the shaking pulse approaches the heteroclinic orbit connecting two unstable standing pulse solutions as d tends to the MX point (see also Fig.3.4 and its caption). This causes the divergence of the period. The traveling pulse loses its stability via period doubling bifurcation at PD point ($d = 0.1305394$), namely the associated Poincare map has Floquet multiplier -1 at this point. If d is slightly smaller than PD point, we observe the chaotic pulse, which implies that the chaotic pulse emerge at the PD point through the **Intermittency Type III route**.

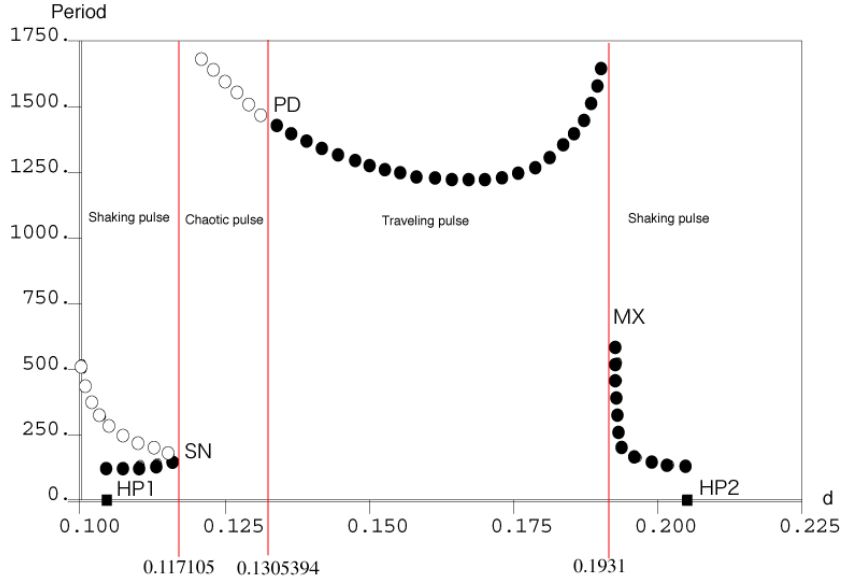


FIG. 4.7. The bifurcation diagram for the branches emanating from the 1 hump solution through the Hopf bifurcations HP1 and HP2. The vertical axis shows the period of the solution. The black disk (resp. white disk) corresponds to a stable (resp. unstable) periodic solution, and SN stands for the saddle-node point. At MX point, the continuation procedure fails because of its long period. The MX point is very close to the value of the emergence point at which the shaking pulse changes into the traveling pulse. The simulation results say that the existence of heteroclinic orbit connecting two unstable standing pulse solution near the MX point (See also Fig.3.4 and its caption). The branch in the middle corresponds to the traveling pulse solution. The period of the traveling solution is the total time where the pulse travel on the ring. The traveling pulse loses its stability via period doubling bifurcation at PD point. The bifurcation at PD point is sub-critical. The unstable periodic branch with double period is not shown in the figure.

5. Interaction among chaotic pulses. In this section we consider the interaction among the chaotic pulses on a lattice. An isolated chaotic pulse is stable to the small perturbation, however when more than two chaotic pulses interact each other, there may be a chance to form an ordered pattern. We first discuss the case for two chaotic pulses, then population of them. It turns out that molecule-like ordered patterns are found numerically, i.e., time-periodic solutions consisting of plural number of oscillating pulses, and creation and destruction of such polymer-like states occur for the population of chaotic pulses.

5.1. Bonding of chaotic pulse (molecule-like structure). Starting from the following initial condition for some positive integer N : $u_i = u_{i+1} = 1.0 + \eta$, $v_i = v_{i+1} = 0.8 + \eta$ where $i = N/3, 2N/3$ and $\eta \in [-0.001, 0.001]$ is a tiny uniform random number, we can obtain two chaotic pulses. When they are well-separated, i.e., N is large, these chaotic pulses move almost independently initially. Because of the chaotic nature of the motion, these pulses come closer at certain time and start to interact each other. Depending on the timing of collision, these pulses fuse into a time-periodic pattern and form a stable molecular-like structure. Here the timing of collision is very important, in fact two chaotic pulses repel each other in most cases. A typical formation process of such a molecular-like state is shown in Fig.5.1 in which we have plotted local maxima as a position of chaotic pulses defined below:

$$(5.1) \quad \psi(t) = \{i \mid i \in \{1, 2, \dots, N\}, u_i(t) - u_{i-1}(t) > 0 \cap u_{i+1}(t) - u_i(t) < 0\}.$$

As is shown in Fig.5.2, 5.3, the molecular-like state is a time-periodic solution with the location of its center of mass being fixed. The resulting ordered state is called 2-molecular pulse.

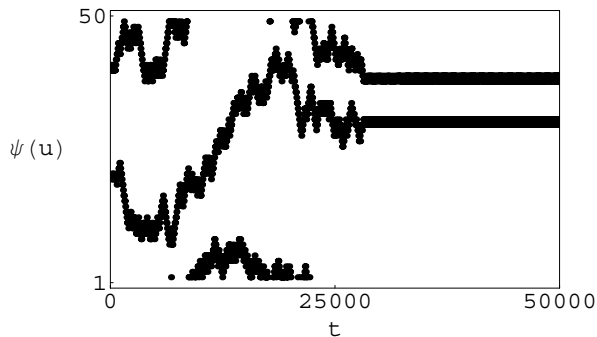


FIG. 5.1. The formation process of a molecular pulse ($d = 0.125$). The space-time position of two chaotic pulses is shown under periodic boundary conditions. These chaotic pulses come closer after some time and interact many times and eventually form a 2-molecular pulse.

Animation file is supplied. formation_molecular.mov.

5.2. Interaction between chaotic and molecular pulses. An isolated molecular pulse is robust and stable to small perturbation, however the introduction of other chaotic pulse might cause the breakup and/or reconstruction of its molecular state through the interaction. Fig.5.4 shows a typical example that a chaotic pulse coming from the right collides with the molecular pulse, forms a 3-molecular state temporarily, and kicks out the left one. Furthermore, as is shown in Fig.5.5, multi-molecular pulse (in this case tetrad-molecule) is formed through collisions. When the

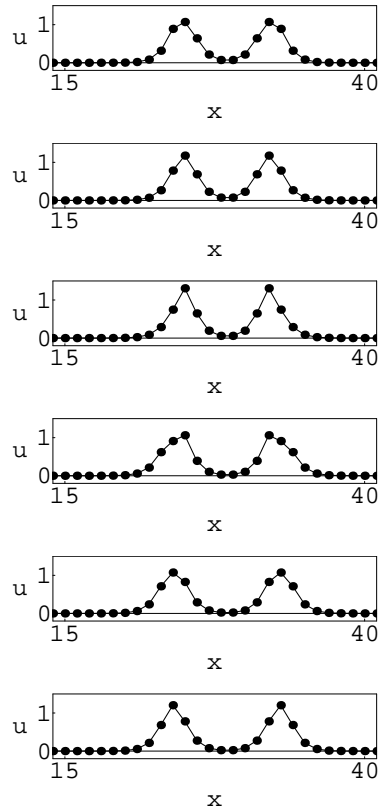


FIG. 5.2. *Snapshots of isolated 2-molecular pulse. Two chaotic pulses collide and form a 2-molecular pulse. Two humps oscillate periodically with in-phase.*

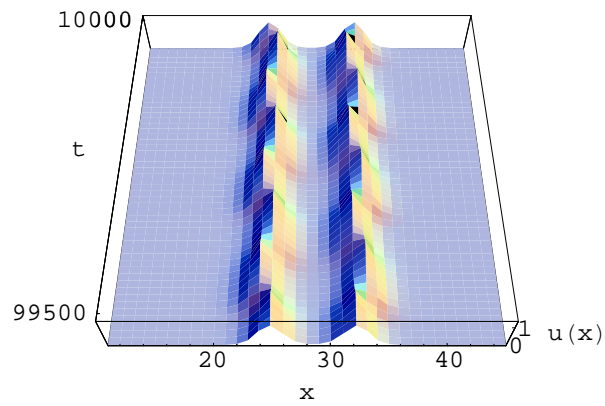


FIG. 5.3. *The birds-eye plot of 2-molecular pulse. Each component of the molecule oscillates with in-phase.*

system size is large enough and many chaotic pulses coexist initially, the evolution of such a system becomes very complex in general as is shown in Fig.5.7: formation and decomposition of molecules and polymers, occur everywhere in the system. It might be interesting to define the rate of the “reaction” of formation and decomposition of molecular/polymer state. The difference of these rates characterize the asymptotic state of the reaction; if the rate of the formation of molecular is larger than that of decomposition, then the system may settle into a non-chaotic state. It is, however subtle thing to determine the life-time (i.e., stability) of molecules or polymers, 2-, 3-molecules, since there are several different types of such ordered states even for the simplest 2-, 3-molecules.

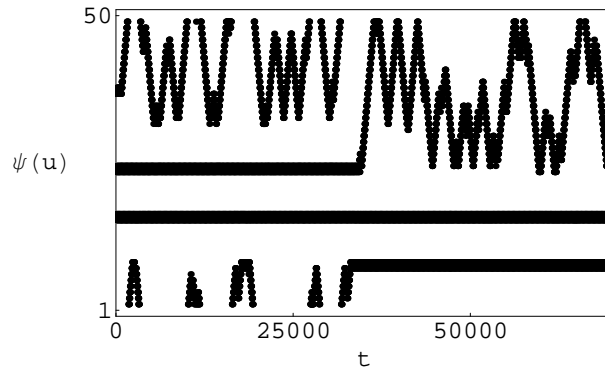


FIG. 5.4. *Collisions of the molecule and chaotic pulses. The space-time position of the molecular and chaotic pulses is shown. A chaotic pulse hits 2-molecular pulse from the left and form a triad-molecule temporarily, then the right one is kicked out and a new molecular is formed.*

Animation file is supplied. `kickout_molecular.mov`.

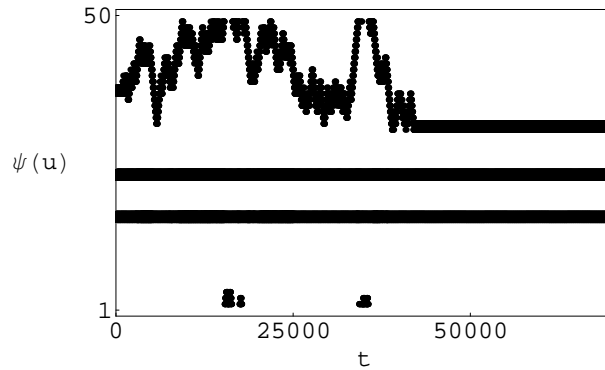


FIG. 5.5. *The formation of polymer. The collision of a chaotic pulse to the 2-molecule causes a formation of a larger molecule like a polymer. The polymer is also a stable periodic solution.*

Animation file is supplied. `formation_trimolecular.mov`.

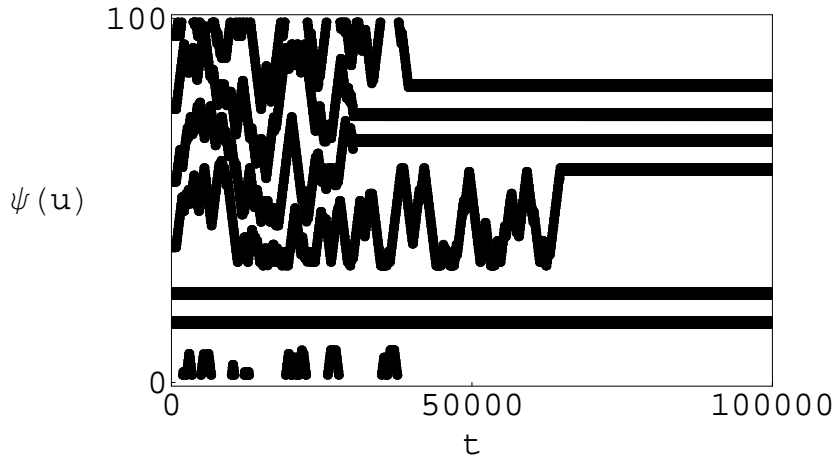


FIG. 5.6. For larger system size, chaotic pulses move randomly initially, collide each other and eventually to form several-molecular structures. The molecular structure sometimes collapse or form a longer polymer by collisions of other chaotic pulse from both sides.

Animation file is supplied. larger1.mov.

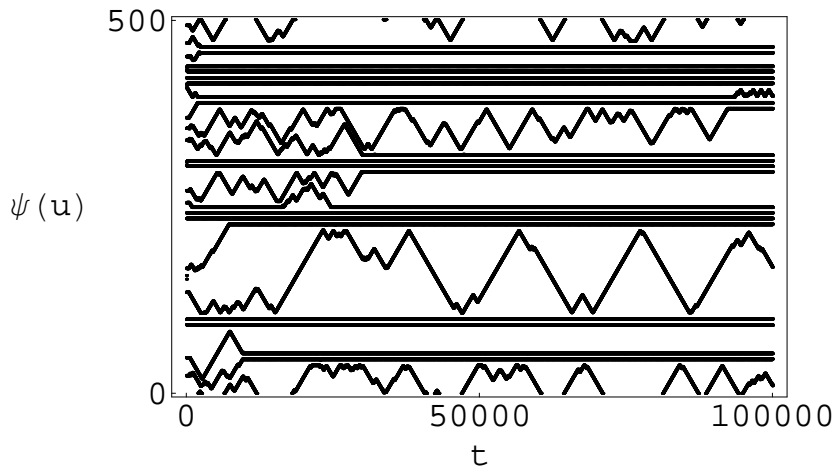


FIG. 5.7. Evolution of population of chaotic pulses. Formation and destruction of polymer-like patterns are observed.

6. Relation to the continuous P-model. In this section, we will discuss about the relation between the discrete P-model and the continuous P-model. In the previous sections, we regard the discrete P-model as an independent model system, not an approximation of the continuous P-model, however suppose that the discrete P-model is regarded as a coarse finite-difference approximation of the original continuous one, then what is a dynamical object when the grid size goes to zero? We shall answer the question for the parameter values in which a chaotic pulse is observed.

6.1. Discretization by finite difference method.

$$(6.1) \quad \begin{cases} \frac{\partial u}{\partial t} = u(u - v^2 - \alpha) + D\nabla^2 u, \\ \frac{\partial v}{\partial t} = ku - v + \beta D\nabla^2 v. \end{cases} \quad x \in (0, L),$$

The P-model (6.1) can be discretized by finite difference method as follows.

$$(6.2) \quad \begin{cases} \frac{du_i}{dt} = u_i(u_i - v_i^2 - \alpha) + \frac{D}{\Delta x^2}(u_{i-1} - 2u_i + u_{i+1}), \\ \frac{dv_i}{dt} = ku_i - v_i + \frac{\beta D}{\Delta x^2}(v_{i-1} - 2v_i + v_{i+1}), \end{cases} \quad i = 1, \dots, n,$$

where Δx is a discretization parameter defined by $\Delta x = \frac{L}{n-1}$. If n is large enough, (6.2) is a good approximation of (6.1). We put d as $d = \frac{D}{\Delta x^2}$, then we have

$$(6.3) \quad D = d\Delta x^2 = d \left(\frac{L}{n-1} \right)^2.$$

We observed the chaotic pulses in previous sections for $d = 0.125, n = 20$ and $L = 1$ ¹. Now, we put these values into (6.3), we get $D = 0.125 \times \left(\frac{1}{20-1}\right)^2 \approx 3.5 \times 10^{-4}$. The parameters where we observe the chaotic pulse for the coarse discretization is $D = 3.5 \times 10^{-4}, \alpha = 0.305, k = 0.95, \beta = 4, L = 1$. In this parameter, we observe a stationary pulse solution as in Fig.6.1(f) for reasonably small grid size. As n is decreased (or the grid size Δx is increased), we first observe a traveling pulse solution as in Fig.6.1(d), then a chaotic pulse solution as Fig.6.1(c). Further decrease of n induces standing pulse as in Fig.6.1(a). The resulting phase diagram with respect to n is depicted in Fig.6.1. Note that the diagram that we have obtained in this section is almost the same as the one obtained by AUTO in Section 4, which is clear in view of the relation (6.3).

In the first section, we mentioned about **pinning** and **propagation failure** phenomenon for the scalar bistable reaction diffusion systems, namely the discretization suppresses the traveling motion. Our results show the opposite case also occurs, namely coarse discretization destabilizes a stationary solution into various moving patterns as in Fig.6.1.

7. Conclusion. We found a new type of localized pulse for the discrete P-model. The pulse changes its position chaotically like a Brownian particle. Employing the strength of interaction among the neighboring sites as a bifurcation parameter, the emergence of such a chaotic pulse was clarified numerically. Type I and Type III intermittencies are responsible for such onset of chaotic behavior. Interaction among the chaotic pulses is quite remarkable, in fact when two chaotic pulses collide with an appropriate timing, then they form a localized oscillatory ordered state called the molecular state. More than two chaotic pulses sometimes form a multi-molecular state called the polymer state. These molecular states are time-periodic and stable, however they may break up through the collisions with other chaotic pulses. This type of localized chaotic pulse may exist for a class of reaction diffusion systems on

¹In fact, the discrete model has no spacial scales. Therefore, L can be arbitrarily chosen.

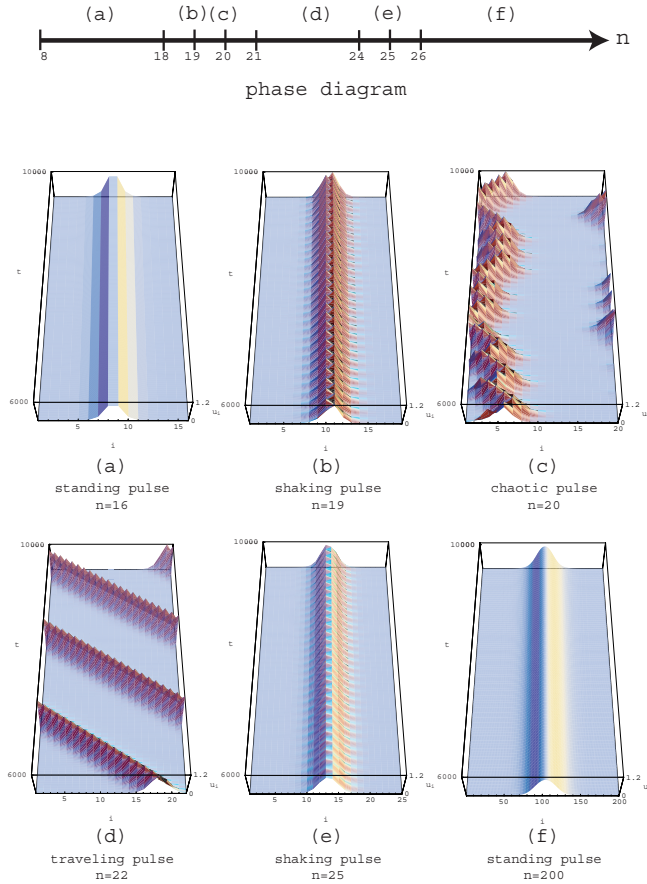


FIG. 6.1. A variety of pulses for the continuous P -model with given grid number n . If n is sufficiently large, the given ODEs becomes a good approximation to the original PDEs. ; (above): A phase diagram for the n compartments discrete P -model subject to periodic boundary conditions. (below): Bird-view plot for each phase. (a)(f) Standing pulse. (b)(e) Shaking pulse. The shaking pulse is a periodic solution that shakes its shoulder with keeping its original position. (c) Chaotic pulse. The chaotic pulse moves chaotically with keeping its localized structure. (d) Traveling pulse. All the other parameters are fixed as $D = 3.5 \times 10^{-4}$, $\alpha = 0.305$, $k = 0.95$, $\beta = 4$ respectively.

a lattice, in fact the discrete Gray-Scott model has such a chaotic pulse, however mathematical characterization for the existence of chaotic pulse remains as an open question.

REFERENCES

- [1] D.G.Aronson, E.J.Doedel, and H.G.Othmer, An analytical and numerical study of the bifurcations in a system of linearly-coupled oscillators, *Physica D*, **25**(1987),20-104.
- [2] J. Bell, *Some threshold results for models of myelinated nerves*, *Math. Biosci.* 54(1981),181-190.
- [3] Shui-Nee Chow and John Mallet-Paret, *Pattern formation and spatial chaos in lattice dynamical systems -Part I and II-*, *IEEE Trans. Circuits and Systems*, **42**(1995), 746-756.
- [4] E. J. Doedel, A. R. Champneys, T. F. Fairgrieve, Y. A. Kuznetsov, B. Sandstede and X. Wang,

- AUTO97: Continuation and bifurcation software for ordinary differential equations (with HomCont)*, <ftp://ftp.cs.concordia.ca/pub/doedel/auto>, (1997).
- [5] T. Erneux and G. Nicolis, *Propagating waves in discrete bistable reaction diffusion systems*, Physica D. **67**(1993),237-244.
 - [6] M. Hildebrand, M. Kuperman, H. Wio, A. S. Mikhailov and G. Ertl, *Self-Organized Chemical Nanoscale Microreactors*, Phys. Rev. Lett. **83** (1999), 1475-1478.
 - [7] J. P. Keener, *Propagation and its failure in coupled systems of discrete excitable cells*, SIAM J.Appl.Math., **47**(3)(1987)556-572.
 - [8] J. P. Keener, *The effects of discrete gap junction coupling on propagation in myocardium*, J. Theor. Biol. **148**(1991)49-82.
 - [9] J. Mallet-Paret, private communication.
 - [10] H. F. Weinberger, *Long-time behavior of a class of biological models*, SIAM J. Math. Anal. **13**(1982),353-396.
 - [11] Y. Nishiura and D. Ueyama, *A skeleton structure of self-replicating dynamics*, Physica D, **130**(1999),73-104.
 - [12] E. Ott, *Chaos in dynamical systems Second Edition*, Cambridge Univ.Press (2002).
 - [13] H. G. Schuster, *Deterministic Chaos*, Physik-Verlag (1984).
 - [14] R. Seydel, *Practical Bifurcation and Stability Analysis:from equilibrium to chaos*, Springer-Verlag (1994).
 - [15] G. Benettin, L. Galgani and L. -M. Strelcyn, *Kolmogorov entropy and numerical experiments*, Phys. Rev. A, **14**(1976), 2338-2345.
 - [16] A. Wolf, J.B. Swift, H.L. Swinney and J.A. Vastano, *Determining Lyapunov exponents from a time series*, Physica D**16**(1985),285-317.
 - [17] Y. Pomeau and P. Manneville, *Intermittent Transition to Turbulence in Dissipative Dynamical Systems*, Comm.Math.Phys., 74(1980)189-197.